



SPE 64374

Numerical Modelling of Capillary Transition Zones

Geir Terje Eigestad, University of Bergen, Norway and John Alex Larsen, Norsk Hydro Research Centre, Norway

This paper was prepared for presentation at the SPE Asia Pacific Oil and Gas Conference and Exhibition held in Brisbane, Australia, 16–18 October 2000.

This paper was selected for presentation by an SPE Program Committee following review of information contained in an abstract submitted by the author(s). Contents of the paper, as presented, have not been reviewed by the Society of Petroleum Engineers and are subject to correction by the author(s). The material, as presented, does not necessarily reflect any position of the Society of Petroleum Engineers, its officers, or members. Papers presented at SPE meetings are subject to publication review by Editorial Committees of the Society of Petroleum Engineers. Electronic reproduction, distribution, or storage of any part of this paper for commercial purposes without the written consent of the Society of Petroleum Engineers is prohibited. Permission to reproduce in print is restricted to an abstract of not more than 300 words; illustrations may not be copied. The abstract must contain conspicuous acknowledgment of where and by whom the paper was presented. Write Librarian, SPE, P.O. Box 833836, Richardson, TX 75083-3836, U.S.A., fax 01-972-952-9435.

Abstract

For a large number of reservoirs, a vertical transition zone between water and oil exists. In this zone, both water saturation and capillary pressure vary with height. Traditionally one assumes that there is a relation between capillary pressure and water saturation, given by a Pc-S primary drainage curve prior to any production in the reservoir. The vertical fluid distribution is found by assuming equilibrium between capillary forces and gravity.

This paper will focus on numerical modelling of the fluid distribution as production is started in a reservoir. As wells may be open and shut during the (field) lifetime of a reservoir, both imbibition and drainage may occur in different parts of a reservoir. The numerical model will take into account the irreversibility of imbibition and drainage, commonly known as hysteresis, which applies for both capillary pressure and relative permeability.

Our test examples will deal with three different production rate regimes; *capillary-dominated*, *capillary-viscous* and *viscous*. We investigate the fluid distribution in the transition zones as the wells are shut down and equilibrium again is reached for the different cases. The tests will show that the fluid distribution differs for different injection- and production rates. For the case where the production in the reservoir is very close to equilibrium, we also show how the fluid distribution can be found analytically.

Introduction

The transition between water and oil is defined as the oil-water contact (OWC) and limits the water zone from the oil zone. Even though the OWC may be given a specific vertical

position by an appropriate definition, the transition between oil and water in natural occurring reservoirs will be diffuse. This diffuse transition is, for many reservoirs, important for reserve estimates and modelling of the connate water distribution. Common for such reservoirs is the fact that the capillary transition zone constitutes a substantial part of the oil zone. This is either caused by low permeability, high interfacial tension or a small density difference between oil and water. Far less investigated, but probably important for many reservoirs, are the transition zones that occur due to chemical processes that locally alter the wettability and a later pre-historic OWC movement herein. It is a common assumption that hydrocarbons found in reservoirs today have migrated from a source at a different location. The oil might then have migrated into a reservoir which was 100% water saturated and had a strong water-wet preference. The process will then correspond to primary drainage.

Since most reservoirs are considered to be water-wet initially, the microscopic distribution of oil is restricted to the larger pores with low capillary pressure. The distribution of water is constrained to smaller pores where the entry-pressure is too large for the non-wetting oil and in films between the pore surface and the oil. The water-wet conditions may change if the water films rupture and polar impurities from the oil attaches on the pore surface. Today, oil-wet or mixed-wet conditions are considered to be occurring in half or more of all reservoirs (Chilinggarian¹⁵). On the larger scale the wettability alteration is determined by permeability and porosity, and on the microscopic scale determined by fluid properties, pore surface mineralogy and roughness. For the reservoir engineer, the largescale properties are most important because these properties are used for modelling the initial water saturation (connate water) in the reservoir. A low permeability region will, on a given vertical level above the OWC, give a higher connate water saturation than a high permeability region. A high water saturation will, in turn, give thick water films and many pores completely filled with water in such a way that polar components from the oil never attach on the surface of the pores. Given the same permeability, a high porosity will indicate that the aspect ratio is high and that some of the pores are large. The permeability is mainly controlled by the narrow pore necks and is rather independent of the larger pore bodies. A lower porosity will indicate a smaller aspect ratio and fewer large pores. Given the same level above the OWC, the water

films will be thinner in the larger pores, leading to a higher possibility that the high porosity regions become more oil-wet than the low as found by Hiekal^{14,16}.

The discussion above hardly questions the grouping of Pc-S functions for mixed-wet reservoirs with the scaling coefficient commonly known as Leverett J-scaling, given by \sqrt{k}/ϕ . However, some evidence indicates that this grouping is less critical when the (large scale) connate water distribution is undisturbed from its original position from primary drainage (Swanson¹⁷). The microscopic wettability alteration itself, would probably not lead to any flow of oil and water on a larger scale than a pore. The reason for this is that the ruptured water films leave the water trapped in meniscus without hydraulic continuity and even though the wettability has changed, the original large scale, strongly water-wet fluid distribution is maintained.

In the simplified examples in this paper, the assumption that the connate water is distributed as a strongly water-wet system, is maintained. The reservoir is therefore initialised by a primary drainage Pc-S function, and the free water level (FWL) is located below the OWC. Capillary forces typical for mixed-wet systems will control a water influx or any other external influences, either in historical times or during production. If the system again reaches equilibrium between gravity and capillary forces, the new distribution reflects the mixed-wet system. The FWL will now be located above the OWC due to the negative capillary pressure associated with oil-wet pores. Between the fossile OWC and the new OWC, a paleo (residual) oil zone will exist where the oil mainly is found as disconnected bubbles in water-wet pores and partly trapped clusters in oil-wet pores as seen in Fig. 2. The examples demonstrate the flowrate sensitivities of such processes in a homogenous reservoir. A recently developed hysteresis model (Skjaeveland¹) is for the first time implemented in a numerical scheme in order to simulate the mixed-wet system.

Analytical description of saturation changes in the transition zone

It will first be demonstrated how it is possible to analytically find the fluid distribution in a reservoir when injection- and production rates are very low. If this is the case, one might assume equilibrium between capillary forces and gravity not only initially, but at all times. For a height, h , above some reference level, the following relationship between capillary pressure, P_c , and h will be valid:

$$P_c = \Delta\rho gh. \quad (1)$$

$\Delta\rho$ is the difference in density between oil and water. All our examples will deal with incompressible fluids, hence this entity will be constant.

As mentioned in the introduction, it is common to assume that the relationship between capillary pressure and saturation

is given by a primary drainage curve. However, the following discussion will be valid for more general initial conditions.

A residual oil zone in a reservoir arises when the OWC is perturbed during the lifetime of a reservoir. The first oil-water contact generated after secondary migration has stopped will be defined *fossil OWC*. It is now possible to examine how the fluid redistributes when the OWC rises due to a water source below the fossile OWC. The definition of a new water-oil contact might not be clear numerically because it is not the depth where residual oil is found, but rather where oil starts getting a percolated structure as discussed in the introduction. It could be defined as the level where one has some small oil-relative permeability value, but this criterium would only be approximate. *Free water level*, FWL, will be the level where $P_c=0$, and could instead be used as a criterium; finding how much FWL has risen during the imbibition process. If we know this distance, it would be equivalent to knowing the capillary pressure drop, which is the same for all cells if equilibrium is satisfied at all times. If analytical expressions for the capillary pressure scanning curves that originate from the primary drainage curve are known, one may calculate the new fluid distribution. Fig. 1 will illustrate the approach: Each cell will experience the same drop in capillary pressure, and if we know the *path* of the capillary pressure drop, ie., we know the Pc-S relationship for each grid cell, the new saturation distribution might be calculated.

We have assumed that all cells are initially found on the primary drainage curve. In the case of water-bottom drive, all cells will experience imbibition when the water injector is opened (and we have an oil producer in the top layer of the reservoir). The path of imbibition is not the same as that of drainage, and will be different for cells on different height-levels of the reservoir. The imbibition curves generated for all cells will be termed *scanning curves*. How these curves are found has been the issue in the papers dealing with hysteresis by Skjaeveland¹, Krieberegg and Heineman⁵ and Killough⁶. These papers outline hysteresis models for both capillary pressure and relative permeability.

Note also that this uniform drop in capillary pressure may indicate that negative capillary pressures can be obtained, and this is fully accounted for in mixed-wet reservoirs¹.

Common for refs. 1 and 5 is the fact that the endpoint of different scanning curves will be different. Immobile oil saturation, S_{or} , is hence a function of the initial condition in addition to the history of the reservoir. This is further outlined in the section of this paper where Skjaevelands hysteresis model is discussed. Fig. 2 sketches how a new saturation distribution is found when the principles mentioned above have been used.

Numerical modelling of saturation changes in the transition zone

This work focuses on numerical modelling of fluid flow in an oil-water transition zone. Much emphasis is put on incorporating correct capillary pressure and relative

permeability description for the whole reservoir; ie., including hysteresis in the numerical models.

Many flow simulators make a Newton-approach for solving the discrete, nonlinear equations that arise when the set of differential equations describing the fluid flow in a porous media, are discretized. Our simulator is based on a fully implicit control-volume formulation, and uses integrated versions of the transport equations for multi-phase flow:

$$m_{\alpha}^n - m_{\alpha}^{n-1} + \Delta t^n \sum_j f_{\alpha j}^n = 0. \quad (2)$$

m_{α} is the accumulated mass of phase α , and $f_{\alpha j}$ is the phase flux through surface number j in the control-volume. n will denote time level. Our numerical examples will deal with two-phase flow, where the two phases are water and oil.

The fluid potentials, and hence pressures, are involved in the expressions for the fluxes. Capillary pressures will be introduced in order to eliminate unknowns, hence special consideration must be taken when accounting for hysteresis in our numerical model. This will be discussed further in the section regarding implementation issues, in light of the hysteresis models to be introduced. For a detailed presentation of the mass balance equations and the terms herein, we refer to Aziz¹¹ or Kleppe⁹.

Hysteresis models

To our knowledge there are several models for hysteresis. Among them we mention Killough⁶, Krieberegg and Heinemann⁵ and Skjaeveland¹. We have chosen to implement Skjaeveland's models in our simulator because of it's structure, consistency and few input parameters needed for a full description of hysteresis. Killough's model is implemented in a commercial simulator, and may be used for comparison with numerical results obtained with Skjaeveland's model. Killough's hysteresis generates capillary pressure and relative permeability curves based on interpolation between primary drainage and bounding imbibition and secondary drainage experimental Pc-S curves.

In Krieberegg and Heinemann's hysteresis model, generation of capillary pressure and relative permeability curves is based on the assumption of shapelike scanning loops. The bounding imbibition and drainage curves are used as 'original shapes' for general scanning loops. Their model is somewhat similar to Skjaeveland's model, but Skjaeveland's model puts the generation of capillary pressure curves into the context of wettability of sandstones in a reservoir.

Note that there are also other methods and models that account for hysteresis. A different entity, the *interfacial area*, is used for describing the fluid-flow in a reservoir in work by Hassanizadeh and Gray¹⁸, and Reeves and Celia¹⁹.

Skjaeveland's model

A brief presentation of the hysteresis model introduced by Skjaeveland and his coworkers will be given here. Models for

both capillary pressure and relative permeability have been developed and are implemented in our inhouse simulator.

Capillary pressure

In Skjaeveland's model¹, capillary pressure correlation and relative permeability for mixed-wet reservoirs is discussed. The correlation for mixed-wet reservoirs is based on simple power laws suggested by Corey and Brooks¹². The relation between capillary pressure and saturation for a completely water wet core is given by the following expression:

$$P_{cd} = \frac{c_{wd}}{\left(\frac{S_w - S_{wr}}{1 - S_{wr}}\right)^{a_{wd}}} \quad (3)$$

c_{wd} is the *threshold pressure*, S_w the water saturation, S_{wr} irreducible water saturation and $1/a_{wd}$ is the poresize distribution index [12]. For mixed-wet reservoirs the idea is now to introduce an *oil term* of the same form as Eq. (3) which would be valid for a completely oil-wet reservoir, sum the two branches and obtain the following general expression for capillary pressure in a reservoir:

$$P_c = \frac{c_w}{\left(\frac{S_w - S_{wR}}{1 - S_{wR}}\right)^{a_w}} + \frac{c_o}{\left(\frac{S_o - S_{oR}}{1 - S_{oR}}\right)^{a_o}} \quad (4)$$

The a 's and c 's are constants and it is assumed that there is one set for imbibition and one for drainage. c_w will be a positive constant, and c_o a negative constant. Note also the labelling S_{wR} and S_{oR} ; this is done because Skjaeveland's approach defines capillary pressure functions restricted to subintervals, and because S_{oR} and S_{wR} vary and are dependent on the history of the reservoir. S_{wR} and S_{oR} will hence be adjustable parameters.

All hysteresis curves for capillary pressure will be based on the equation above. If imbibition is started out from irreducible water saturation, S_{wr} , given from Eq. (2), the curve will scan down to irreducible oil saturation, S_{or} . This curve will be denoted the bounding imbibition curve. If (secondary) drainage is started out from S_{or} , the curve will scan back to S_{wr} , (with a different path than the imbibition curve). This curve will be termed the bounding drainage curve. The two bounding curves will cross $P_c=0$ for different saturations. These two saturation values will be input parameters in the model, and define the wettability of the reservoir^{1,8}. Following the terminology of Skjaeveland, the two points will be denoted S_{woi} for imbibition and S_{wod} for drainage. For a further discussion of this, we refer to Morrow⁸ and Skjaeveland¹.

As mentioned in the discussion of analytical solutions, it is common to use a primary drainage capillary pressure curve to describe the initial state of a reservoir prior to production. For primary drainage, Eq. (1) will be used, and the water saturation is allowed to vary between S_{wr} and 1.0. If imbibition

starts when production of the reservoir is started (eg. water bottom drive), a reversal occurs on the primary drainage curve, and the capillary pressure will be given by an *imbibition scanning curve*. This curve will scan towards a residual oil saturation, $S_{oR}[1]$, which is a fraction of S_{or} , determined by *Lands relation*⁷:

$$\frac{1}{S_{oR}[1]} - \frac{1}{S_o[1]} = C. \quad (5)$$

$S_o[1]$ is the oil saturation for the departing point on the primary drainage curve, and C is Land's trapping constant.

C is related to a specific sandstone, and may be found using Eq. (5) when starting out from irreducible water saturation. The capillary pressure curve will then scan towards S_{or} , and the constant is given by Eq. (5). The algorithm for determining the scanning curves for general starting points on the primary drainage curve is given in Ref. 1.

Hysteresis is also allowed between the imbibition curve and a new drainage curve. This curve will be termed a *drainage scanning curve*, and will follow a different path than the (first) imbibition curve, back to the reversal point on the primary drainage curve. This is based on the principle of closed scanning loops, and has been used by several authors such as Kriebernegg and Heinemann⁵. Hysteresis will also be accounted for if a reversal from the drainage scanning curve occurs. A new imbibition scanning curve will be generated, and will again follow a different path than the foregoing drainage curve back to the starting point for the drainage scanning curve. Multiple reversals are allowed, and a procedure for generating general scanning curves is discussed in detail in Skjaevelands original paper.

When solving discrete equations, the hysteresis logics will apply to all grid cells of the reservoir. For the example of water bottom drive, all grid cells will have their starting point for imbibition scanning curves on the primary drainage curve, but this point will be different for cells on different height levels. Depending on what happens with the reservoir, reversals of processes for each individual cell might occur as the fluids flow in the reservoir. The inhouse simulator will systematically generate and save the parameters that are needed for the possible scanning curves for all individual grid cells.

A typical example of a primary drainage curve together with some of its possible scanning curves is depicted in Fig. 3.

Relative permeability

The hysteresis logics has been extended to account for relative permeability in work done by Kjosavik^{3,4}. The main principle here is to use the two branches of the capillary pressure function as weights for calculations of relative permeabilities. The procedure of generating scanning curves for relative permeability is very similar to that of capillary pressure.

As a motivation for deriving general functional relationships for relative permeability, Kjosavik looks at Corey-Burdine expressions for drainage and imbibition of the two fluids in completely water-wet and oil-wet systems respectively. The general capillary pressure equation, Eq. (4), consists of a water branch and an oil branch. For a completely waterwet medium one uses the water branch of the capillary pressure to derive the two Corey-Burdine expressions for drainage water- and oil relative permeability respectively:

$$k_{rwwd} = S_{nw}^{3+2a_{wd}}, \quad (6)$$

$$k_{rowd} = (1 - S_{nw}^{2a_{wd}+1})(1 - S_{nw})^2, \quad (7)$$

where S_{nw} is the normalized saturation, given by

$$S_{nw} = \frac{S_w - S_{wr}}{1 - S_{wr} - S_{or}}. \quad (8)$$

a_{wd} is the same parameter that was introduced in the discussion of capillary pressure, Eq. (3). For drainage in a completely oilwet system, one uses the oil branch for deriving similar expressions for oil relative permeability, k_{rood} , and water relative permeability, k_{rwwd} . Note that we then arrive with 4 expressions for drainage, and that the same must apply for imbibition.

In a mixed wet reservoir it is suggested to make a weighting of the waterwet and oilwet relative permeability functions with the water branch and the oil branch of the capillary pressure function to arrive with

$$k_{rwd} = k_{rw}^0 \cdot \frac{P_{cwd} \cdot k_{rwwd} - P_{cod} \cdot k_{rowd}}{P_{cwd} - P_{cod}}, \quad (9)$$

for mixed-wet drainage relative permeability of water. k_{rw}^0 is the value of the bounding relative permeability curve at S_{or} . For mixed-wet drainage oil relative permeability, we similarly get:

$$k_{rod} = k_{ro}^0 \cdot \frac{P_{cwd} \cdot k_{rowd} - P_{cod} \cdot k_{rood}}{P_{cwd} - P_{cod}}. \quad (10)$$

k_{ro}^0 is the value of the bounding relative permeability curve at S_{wr} . If index d is substituted by i , Eq. (9) and (10) are valid for imbibition processes.

Relative permeability hysteresis

For a thorough presentation of the procedure for generating relative permeability scanning curves, we refer to the paper by Kjosavik⁴. A general procedure for generating relative permeability scanning curves is given here, and it is consistent with the procedure for capillary pressure.

The numerical examples to be discussed mainly deal with processes that have been reversed 2 times or less. We therefore only discuss the procedure briefly for the first two reversals. The principles for general reversals and scanning curves are however easily implemented in the light of the procedure for capillary pressure.

First reversal: Suppose that a reversal of the process occurs at some point $S_w[1]$ on the primary drainage curve, and that an imbibition process is started. The relative permeability curves (one for oil and one for water) will then scan towards the same value $S_{or}[1]$, as that of capillary pressure. For oil, the imbibition curve and the original (primary) drainage curve must have the same value at the reversal point. At $S_{or}[1]$, the imbibition scanning curve will be zero. In Kjosavik's paper the general expressions for relative permeability scanning curves have two adjustable parameters, hence the imbibition scanning curve is now uniquely determined by these two constraints. It should also be mentioned that the two equations to be solved (to determine the adjustable parameters) are linear, which makes them easily solved analytically (2*2-system). Analytical expressions are given in Ref. 4. For the water relative permeability scanning curve, two similar conditions apply, and they are sufficient to determine the scanning curve.

Second reversal: When a reversal occurs for some water saturation value $S_w[2]$ on the first imbibition curve, both the water and oil (drainage) scanning curves will scan back towards $S_w[1]$, and hence be restricted at both points. Since each curve has two adjustable parameters, they will again be uniquely determined by the two imposed constraints.

Figs. 4 and 5 show relative permeability curves for two cases with different distance between reversal points, but otherwise equal curve-parameters. The difference between the imbibition- and the drainage scanning curve is more significant when the distance between the two reversal points is larger. In laboratory measurements, Braun and Holland¹³ find these curves to be reversible, but experimentally differences like those seen in figs. 4 and 5 would be hard to detect with measurements as discussed in Ref. 4. Depending on the distance between the reversal points, it seems that the curves can be approximated to be reversible for numerical purposes in many cases. It should be added that the difference between the imbibition and drainage curves will also depend on the curve-parameters (a's and c's), but we have not performed any analysis for deriving criteria for accepting the curves as reversible.

Implementation issues

In order to make Newton's method converge for the nonlinear set of equations arising from Eq. (2), the functions involved in the equations should have Lipschitz continuous derivatives. As seen in the models introduced for Pc-S and kr-S hysteresis, such conditions might however not be satisfied at inflection points. Moreover, when the simulator iteratively

solves for saturations, the iterations are not likely to be monotoneous, and the sequence of updated saturation values might indicate that hysteresis has occurred. This might merely be a numerical effect, and must be distinguished from real hysteresis.

We suggest an approach where we don't change capillary pressure and relative permeability curves during a timestep, but update the direction of each cell after the timestep has converged.

During one timestep, it will be assumed that the processes have a monotone direction, ie., either imbibition or drainage occurs for a specific grid cell in that timestep. When simulating from timestep n to $n+1$, we do not necessarily know what happens for a process in between the two time levels. If, after convergence of the timestep, the saturation-change during that timestep was opposite to what was assumed, we only know that the saturation has gone through a stationary point in this time step or the foregoing time step. The grid cell(s) which this is the case for is/are on a new hysteresis scanning curve. In our approach we have chosen to accept the result for the timestep if the saturation change (absolute value) was less than some \mathcal{E} , and use the updated saturation as the reversal point for the scanning curve starting out when the process is reversed. Neither this saturation value nor the saturation value from the previous timestep is the *correct* value for the reversal point, so this is the approximation that must be made when we only know that a reversal occurs in specific timesteps. Our method can then be viewed as predetermined for the directions of the processes, but still fully implicit for all other variables. It can be argued that choosing the saturation value at the previous timestep would be a more accurate guess for the reversal point, but this is reflected in \mathcal{E} , (normally 10^{-3}).

The error in capillary pressure and derivatives due to this approximation will be smaller and smaller as the curve scans back towards the previous reversal point due to the closed scanning loops. This is seen as a 'damping effect' if the process does not change direction again as in Fig. 5.

The approximation made here might be viewed as a *one-sided smoothing process* in order to make the curves have continuous derivatives at all timesteps. This ultimately makes the code for simulating displacement processes more stable. For future work, the problem of finding inflection points should be investigated, and this might be possible to formulate mathematically and incorporate in the algorithm.

Results and discussion

The test cases to be examined here will deal with fluid flow mainly vertically in a homogeneous reservoir. A water injector is located in the bottom of a rectangular, synthetic reservoir, and an oil producer is located in one of the upper grid cells of the reservoir. This is commonly known as water bottom drive. For numerical calculations, a uniform grid is used.

The reservoir is assumed to be mixed-wet, and the input data describing the hysteresis and wettability in the context of

refs. 1 and 4 is listed in the Appendix. The parameters listed there will show that imbibition scanning curves are very steep near their origin on the primary drainage curve. Due to experimental data, which shows nearly vertical scanning curves, we consider it important to simulate examples that exhibit these patterns.

The height of the reservoir is 200 m. In the bottom there is a 50 m water zone (100% water saturated), and above the OWC, the transition zone is located. It should be mentioned that although the transition zone might seem exaggerated, the water saturation in the upper part of the transition zone will be close to S_{wr} .

We use the standard assumption that the initial fluid distribution is found by assuming equilibrium between capillary and gravitational forces and that the relation between capillary pressure and saturation is given by a primary drainage curve.

Three different production rate regimes will be simulated; capillary-dominated, capillary-viscous and viscous. This is done, by going gradually from low rate to high rate. The injection well and the production well will have the same rate, and will be shut down as approximately half of the oil in the reservoir has been produced. Depending on the rate, the fluids will redistribute until equilibrium is reached again.

The examples are synthetic and simple, yet exhibit many important aspects of fluid flow simulation when accounting for hysteresis.

Low rate

The first test case will be an example of capillary-dominated flow. The injection and production rates are low, and the solution should be close to an analytical solution, which can be obtained based on the discussion earlier. How close the solution is to the analytical solution will be discussed when compared with an *ultralow rate* example.

The rates are 0.004 cm per day (1.46 cm per year), and the wells will be shut off after 0.15 porevolume water and oil have been injected and produced respectively. The fluid distribution and capillary pressure development are depicted in figs. 7 and 10 respectively.

When the wells are open, this is an example of pure imbibition. After well shut off, only gravity and capillary forces are driving forces of the system. From Fig. 10 it is seen that there is a (very nearly) linear relationship between capillary pressure and height at an intermediate time level of production, but at well shut off this has been slightly altered. This is most apparent for the cells in the bottom of the transition zone, and may be explained by very small relative permeabilities for oil (10^{-7} - 10^{-8}). The water will not be able to sweep enough oil to have equilibrium here, and hence invade the middle zone. The effect is seen from the fact that the capillary pressure has dropped more in the middle zone at shut off. Even the small flow rates for this regime are not small enough to maintain equilibrium at the last stage of production.

The water has swept much oil in the lower part of the transition zone, and the front is steep at well shut off. The

shape of the front will depend strongly on the imbibition scanning curves, as well as the production rates (related to Buckley Leverett with capillary forces and gravity, see for example Ref. 10). As mentioned above, the imbibition scanning curves are very steep here, and this will explain the front obtained for this case since we are close to the equilibrium solution. Notice also that the front is smoothed near its top (height). This is an effect of capillary pressure and the solution being close to the analytical solution. In the top of the transition zone, the grid cells have felt (almost) the same capillary pressure drop as the cells lower in the reservoir. Note, however, that the saturation changes are almost negligible. This is because of the very steep imbibition scanning curves that these cells will follow near S_{wr} .

To reach equilibrium after shut off, the cells in the lowermost layer of the transition zone must continue imbibition. Mass balance and deviation from equilibrium force some of the water in the middle layer to move back down into the lower layer. For the upper part of the transition zone, a very small decrease of capillary pressure is needed to reach equilibrium. The Pc-h relation in the reservoir at 1 million days (simulation stop) has been plotted, and the relationship is nearly linear except for a small deviation in the bottom layer. For saturations, however small changes are seen from well shut off until equilibrium is reached.

Medium rate

The medium rate case is a case of capillary-viscous flow. The rates are 100 times higher than the low rate example (1.46 m per year), and the same porevolume is injected and produced as for the low rate case. Numerical results are depicted in figs. 8 and 11. As seen from the capillary pressure development, the fluid flow has taken place further away from equilibrium than for the capillary dominated flow. The water column is thinner than the low rate example; water sweeps less oil, and moves further up in the reservoir. This is seen by the lower drop of capillary pressure near the middle of the transition zone at well shut off.

After the wells have been shut off, a redistribution of the fluids must occur. The picture is similar to the low rate example, but the effects are much more apparent. In the bottom layer of the transition zone, imbibition will continue, in the middle layer imbibition will stop and drainage will take place. For the top layer, imbibition will also continue. The capillary pressure must increase more in the middle zone than earlier, and this is reflected in the larger saturation difference from shut off until equilibrium is reached.

High rate

For higher injection and production rates, the fluid flow will be viscously dominated. Rates are 10 000 times bigger than the low rate case (146 m per year), and the same porevolumes are injected as before. Numerical results are depicted in figs. 9 and 12. The fluid flow has occurred even further away from equilibrium; this is very apparent from the

capillary pressure plot. The water front has moved higher up in the the reservoir and less oil has been swept in the lower part of the transition zone. Also, the front is less smeared than the low-rate example. After shut off, the redistribution processes follow the same trends as before. Due to the larger deviation from equilibrium while wells were open, capillary pressure changes from shut off until equilibrium is reached are bigger. This again leads to larger saturation changes to reach equilibrium.

It should be commented on the ‘small front’ that does not move down in the reservoir again after the wells have been shut off. This is a consequence of the drainage curves that apply for processes that are reversed from imbibition processes. If the simulator didn’t account for hysteresis between the first imbibition process and a new drainage process, the saturation distribution at equilibrium would be different. If the distance between the reversal points is small and $P_c > 0$ at the reversal, a relatively large capillary pressure increase is needed to change saturations significantly.

If the distance between the reversal points is bigger and $P_c < 0$ for the specific cell, the drainage curve is more similar to the imbibition curve, and an increase of capillary pressure has a greater effect on saturations. How close the (second) reversal point is from the oil branch asymptote must also be taken into consideration when looking at the effect a capillary pressure change has on saturations.

Comparison to equilibrium solution

How the fluid distribution at shut off deviates from a reference solution will now be discussed.

The capillary pressure development has so far been used to understand and validate the trends seen for saturation changes after the wells have been shut off and as we approach equilibrium again. The examples of increasing rates show the trends in the solution at well shut off. For the water front, more smearing is seen for lower rates. The front in Fig. 7 is steep, but some smearing is seen for it’s upper part (height).

Ideally, one would compare the results at well shut off with an analytical solution. As mentioned above, this solution can be obtained when we know the uniform drop in capillary pressure for all grid cells in the reservoir. For the test case, we do however not know exactly how much the pressure will drop when a certain amount of water is injected in a reservoir, even when equilibrium is satisfied at all times.

As a way of comparing the numerical results for the test cases with a reference solution, we have chosen to simulate a test case with ultralow rate; 1/10 of the rates of the low rate case. The capillary pressure development will show that this rate regime is closer to equilibrium than the low-rate case, and saturation changes from well shut off until equilibrium is reached, are smaller than 0.0001 for all grid cells.

The relative deviations from the reference solution for saturation distributions at shut off have been plotted in Fig. 13 for different rates.

As seen from the figure, the deviation is largest near the position of the new FWL, and increases as rates increase. This

can be explained by the fact that scanning curves will have inflection points (double derivative=0) near the saturations that coincide with $P_c=0$. At these points, only a small change of capillary pressure may lead to large changes in saturation.

Compressed transition zone

The three rate-regimes above have also been simulated with a more compressed transition zone. The only parameter that needs to be adjusted in order to have a more compressed zone, is a_{wd} . The new examples will have a transition zone where the water saturation is less than 0.8% away from S_{wr} 50 m above fossil FWL.

The same trends as for the first transition zone are seen for the simulations, and relative deviations from the reference solution (with $a_{wd}=0.5$) are depicted in Fig. 14.

Comparison to Killough’s hysteresis model

The same test examples have been simulated with a commercial simulator, where Killough’s hysteresis model is implemented. As input for this simulator one must give the primary drainage curves and the bounding imbibition and secondary drainage curves for both capillary pressure and relative permeability. These curves are generated with the same input as was used for Skjaeveland’s model, and use the same curve parameters as in the Appendix. There is, however, one major difference between the two codes. The inhouse simulator uses analytical expressions for capillary pressure, relative permeability and it’s derivatives, whereas the commercial simulator uses tables and linear interpolation between input values.

The saturation distributions at different time levels have been plotted in figs. 15-17 for increasing rates for the first transition zone. The plots show the same trends as the results for Skjaeveland’s model in the lower part of the transition zone. In the upper part, however, some differences are apparent. For the low rate case, Fig 17, the process has been close to equilibrium, but much more capillary diffusion is seen in the top of the reservoir than was obtained by Skjaeveland’s model. This may be explained by following:

When plotting scanning curves for different grid cells, we see that they are not as steep as those obtained for Skjaeveland’s model. This means that the same capillary pressure drop will affect saturations differently in the two models.

We know that Killough’s model has been modified in the simulator, and the fact that the scanning curves are less steep might be an effect of the modification and the algorithm for generating scanning curves as well. Also, since the simulator uses linear interpolation between points in the table for saturations and capillary pressure, this might give less steep scanning curves near the water asymptotes. We have tried to use more (saturation) points as input in the commercial simulator to check this, but convergence problems are then seen.

For the low-rate case, results show that the cells in the upper part of the transition zone have not felt the same

capillary pressure drop as the cells lower in the reservoir. After well shut off, imbibition must continue in the upper cells, and a much more significant saturation increase is seen here than in Fig. 7. It then seems like the process has been closer to equilibrium when Skjaeveland's hysteresis model had been accounted for.

The medium- and high rate examples show less capillary diffusion in the upper part of the reservoir than for low rates, as expected. After well shut off, the fluids redistribute, and the scanning curves are important for understanding what happens in order to reach equilibrium. Capillary pressure plots show that the capillary pressure has decreased very little in the upper part of the transition zone during production. After shut off, imbibition must continue in order to reach equilibrium, and this is seen as a significant saturation increase in the upper part both for medium- and high rates. This is in contrast to the results obtained for Skjaeveland's model.

Relative deviations from an ultralow solution are depicted in figs. 18 and 19 for the first transition zone and the compressed transition zone respectively. The deviation from ultralow rate is much smaller for the upper grid cells for the compressed transition zone, whereas plots for Skjaeveland's model showed negligible differences for both transition zones.

Adjusted hysteresis parameters

The imbibition scanning curves are important for the water front for capillary dominated flow. Results for Skjaeveland's model have shown that there is more smoothing near the top of the water front for capillary dominated flow than for viscously dominated flow. The effect is still not seen in the upper grid cells as mentioned earlier. As was pointed out, one of our main intentions was to simulate processes with steep imbibition scanning curves. The curve parameter that is most important for imbibition from primary drainage is a_{wd} . When it is increased, less steep scanning curves are obtained. We have run the same test examples as before with this parameter adjusted to 0.4, and saturation distributions at well shut off for the different rates have been plotted in Fig. 20.

For the low rate example, the effect of capillary diffusion is much more apparent than previously. The front for the low rate case (2) is very similar to the water front for the the low rate case run on the commercial simulator, where Killough's hysteresis model was used. It seems like the input parameters for Skjaeveland's hysteresis model can be tuned, in order to reproduce the results that were obtained for the commercial simulator. The reason for this is probably that the scanning curves then become more similar, but we have not performed any systematic analysis of this.

For medium- and high rates, the effect of capillary smoothing is not seen at shut off, and is again explained by the deviation from equilibrium.

Conclusions and further work

This paper has focused on simulating the fluid distribution in vertical capillary transition zones. Skjaeveland and Kjosavik's models for capillary pressure and relative permeability have been implemented in a simulator to incorporate hysteresis.

Numerical results obtained for water bottom drive at different rates, have been compared with a reference solution. The reference solution is representative for an analytical approach of finding the fluid distribution in a reservoir under certain assumptions. The results show that the largest deviation from the reference solution for test cases with higher injection and production rates, is found near FWL.

Skjaeveland's model and Killough's model may give different results with the same bounding curves. Tuning the curve parameters in Skjaeveland's model while keeping the input for Killough's model fixed, seem to make the difference between the results for the two models smaller.

The methods presented here could be extended to more complex test cases. A nearlying example to investigate is a layered reservoir, where the different layers have different capillary pressure and relative permeability functions. Extension to 3-phase flow could also be investigated, and maybe follow the lines of Kriebeneegg and Heinemann⁵, where three-phase relative permeabilities are obtained bases on Stone's²⁰ models .

Nomenclature

a	= constant, dimensionless
c	= constant, psi, bar or mbar
C	= Land's trapping constant
k	= relative permeability, dimensionless
Pc	= capillary pressure
S	= saturation
$Pc-S$	= capillary pressure as function of S
$kr-S$	= rel. perm as function of S

Subscripts:

c	= capillary
d	= drainage
i	= imbibition
w	= water
o	= oil
r	= residual or relative
n	= normalised
α	= phase; oil or water
0	= zero point

Superscripts:

n	= time-level
-----	--------------

0 = endpoint

Acknowledgements

We would like to thank Svein Skjaeveland, Ivar Aavatsmark and Gunnar Fladmark for useful help in this work. We would also thank the management of Norsk Hydro for allowing us to publish this paper.

References:

- Skjaeveland, S.M., Siqveland, L.M., Kjosavik, A., Hammersvold, W.L., and Virnovsky, G.A.: "Capillary Pressure Correlation for Mixed-Wet Reservoir", SPE 39497 presented at the 1998 SPE India Oil and Gas Conference, New Delhi, India, April 7.-9.
- Brooks, R.H. and Corey, A.T.: "Hydraulic Properties of Porous Media", Hydraulic Paper No. 3, Colorado State U., 1964.
- Kjosavik, A.: "Integrated Modelling of Relative Permeability and Capillary pressure". M.Sc. Thesis, Stavanger College, Norway (1999).
- Kjosavik, A., Ringen, J.K., Skjaeveland, S.M.: "Relative Permeability Correlation for Mixed-Wet reservoirs", SPE 59314, presented at the 2000 SPE/DOE Improved Oil Recovery Symposium held in Tulsa, Oklahoma, 3.-5. April 2000.
- Kriebernegg, M., and Heinemann, Z.: "A new Model for History Dependent Saturation Functions in Reservoir Simulation". Paper presented at the 1996 European Conference on the Mathematics of Oil Recovery, Leoben, Austria, 3-6. Sept.
- Killough, J.E.: "Reservoir Simulation with History Dependent Saturation Functions". SPEJ (February 1976) 16, 37; Trans., AIME., 261.
- Land, C.S.: "Calculation of Imbibition Relative Permeability for Two- and Three-Phase Flow from Rock Properties". SPEJ (June 1968), 8, 149; Trans., AIME., 243.
- Morrow, N.R., "Wettability and it's Effects on Oil Recovery". JPT (December 1990) 42, 1476; Trans., AIME., 289.
- Kleppe, H.: "Fundamental Reservoir Simulation". Teaching material, Stavanger College, Norway.
- Collins, R.E.: "Flow of Fluids Through Porous Materials". PennWell Publishing Company, Tulsa, Oklahoma.
- Aziz, K. and Settari, A.: "Petroleum reservoir simulation". Elsevier Applied Science Publishers, London, England 1985.
- Standing, M.B.: "Notes on Relative Permeability Relationships". Proc., University of Trondheim, NTH, Norway (1975).
- Braun, E.M. and Holland, R.F.: "Relative Permeability Hysteresis: Laboratory Measurements and a Conceptual Model". SPERE (Aug. 1995) 222-28.
- Elshahawi, H., Fathy, K. and Hiekal, S.: "Capillary Pressure and Rock Wettability Effects on Wireline Formation Tester Measurements". SPE 56712, presented at the 1999 SPE Annual Technical Conference and Exhibition, Houston, Texas, 3-6. October 1999.
- Chilingarian, G.V. and Yen, T.F., "Some notes on Wettability and Relative Permeability of Carbonate Rocks", Energy Sources Vol. 7, No. 1 (1983), pp 67-75.
- Hiekal, S., Kamal M., Hussein, A., Elshahawi, H.: "Time Dependence of Swept Zone Remaining Oil Saturation in Mixed-Wet Reservoirs", paper presented at SPWLA, Japan, 24-25 September, 1998.
- Swanson, B.F., "Rationalizing the influence of Crude Wetting on Reservoir Fluid Flow With Electrical Resistivity", Journal of Petroleum Technology (August 1980), p. 1459-1464.
- Hassanizadeh, S.M. and Gray, W.G.: "Thermodynamics Basis of Capillary Pressure in Porous Media". Water Resour. Res. 29 (1993) 3389-3405.
- Reeves, P.C. and Celia, M.A.: "A Functional Relationship between Capillary Pressure, Saturation and Interfacial Area as revealed by a Pore-scale Network Model". Water Resour. Res. 32 (1996) 2345-2358).
- Stone, H.L.: "Probability Model for Estimating Three-Phase Relative Permeability", JPT (Feb. 1970), Trans., AIME. Vol. 249, pp. 214-218.

Appendix: Reservoir data

The data and parameters describing the reservoirs and the hysteresis are given here:

Grid and fluid data

Grid size:	3*1*57
Dx:	33.3m
Dy:	20.0m
Dz:	3.50m
Permx:	200mD
Permz:	200mD
Porosity:	0.20
Density, wat:	800kg/m ³
Density, oil:	1000kg/m ³
Oil visc:	0.24
Wat. visc:	0.32

Hysteresis/Wettability:

S _{or} :	0.25
S _{wr} :	0.20
c _{wd} :	0.10
c _{wo} :	0.10
a _{wd} :	1.00
a _{od} :	0.25
a _{wi} :	0.25
a _{oi} :	0.50
S _{w0i} :	0.50
S _{w0d} :	0.70

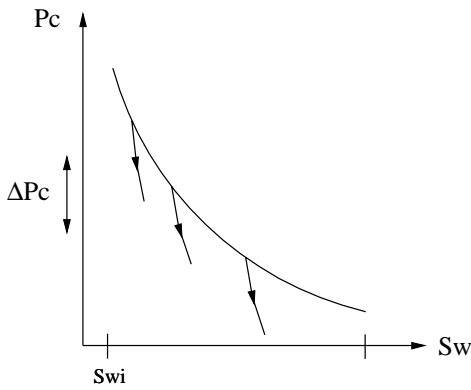


Fig. 1: If the same saturation drop/increase is felt everywhere in the reservoir, an analytical saturation distribution solution may be found.

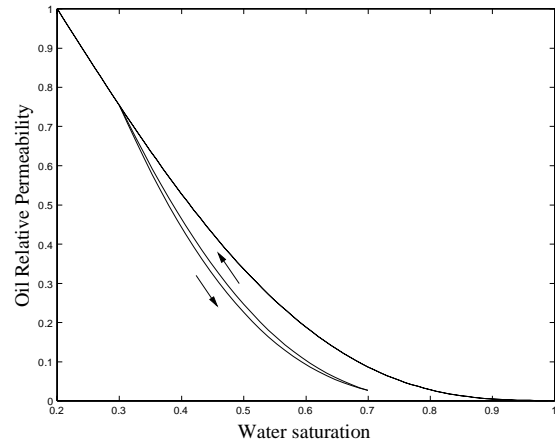


Fig. 4: Oil relative permeability imbibition and drainage scanning curves plotted together. Imbibition scanning curve has its starting point on primary drainage curve.

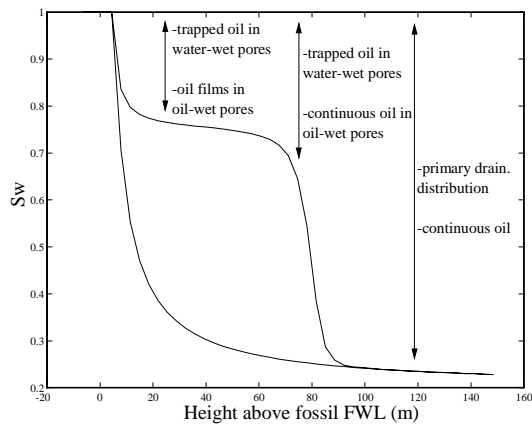


Fig. 2: Saturation distribution initially and after the OWC has risen.

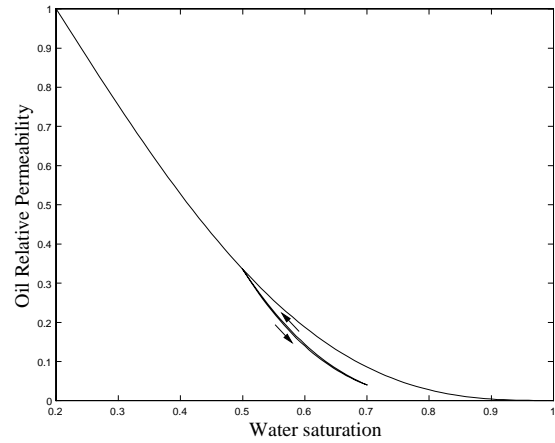


Fig. 5: Relative permeability imbibition and drainage scanning curves plotted together. The distance between the reversal points is small, and the curves are hard to distinguish.

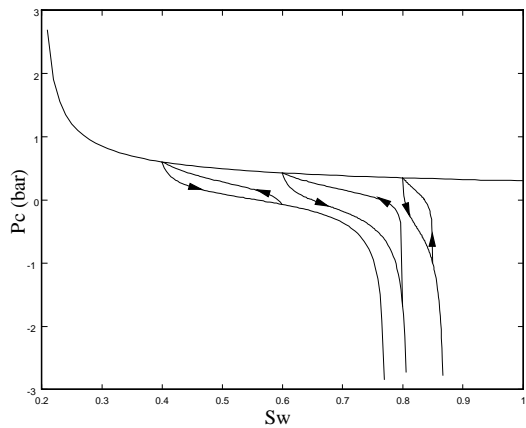


Fig. 3: Primary drainage capillary pressure curve together with imbibition and drainage scanning curves.

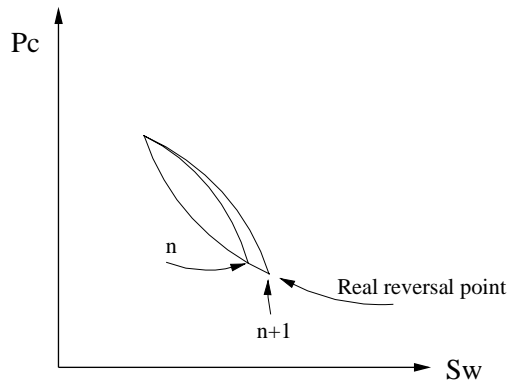


Fig. 6: The effect of not choosing the correct inflection point for drainage scanning curve is decreasing due to the closed

scanning loops.

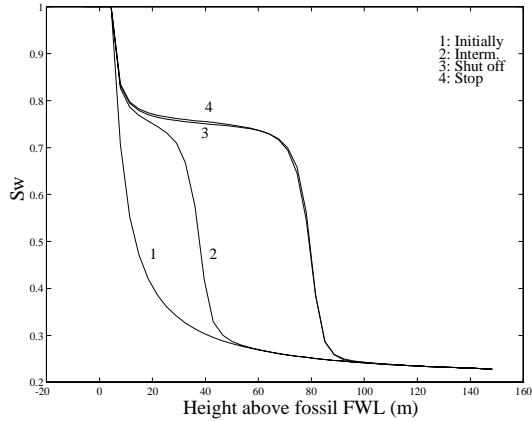


Fig 7: Saturation distribution at different time levels for low rate Case. Intermediate is 50.000 days, and shut off is at 150.000 days.

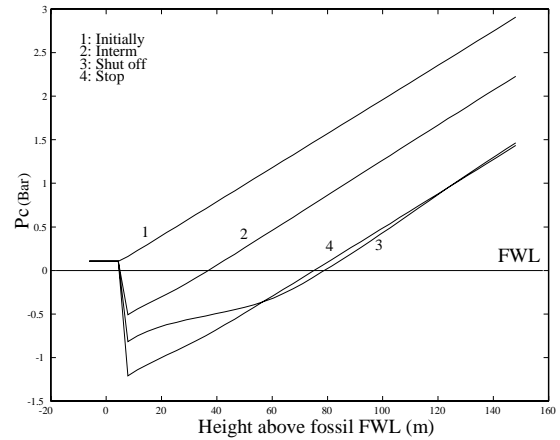


Fig. 10: Capillary pressure development, low rate case.

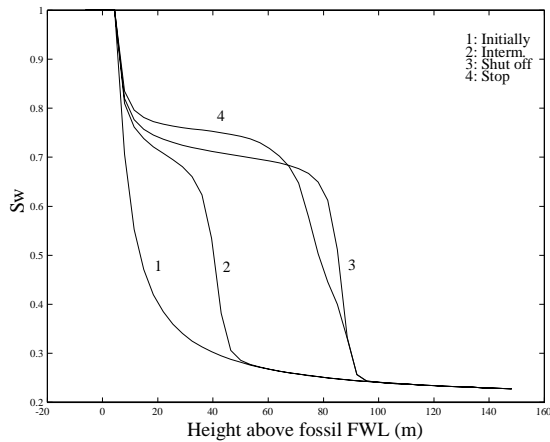


Fig 8: Saturation distribution at different time levels for medium rate case. Intermediate is 500 days, and shut off is at 1.500 days.

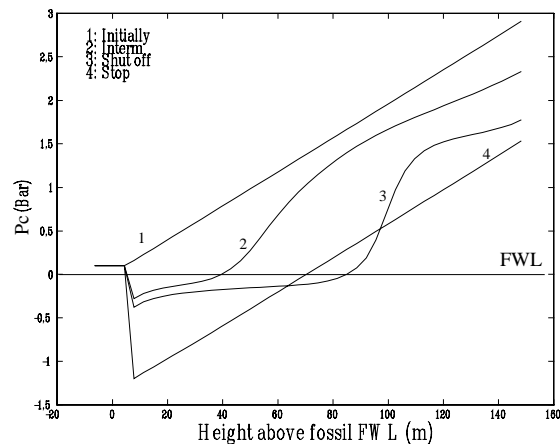


Fig. 11: Capillary pressure development, medium rates.

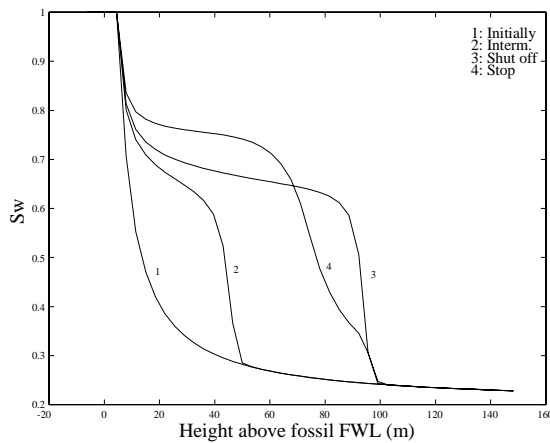


Fig 9: Saturation distribution for high rate case. Intermediate is 5 days, shut off is at 15 days.

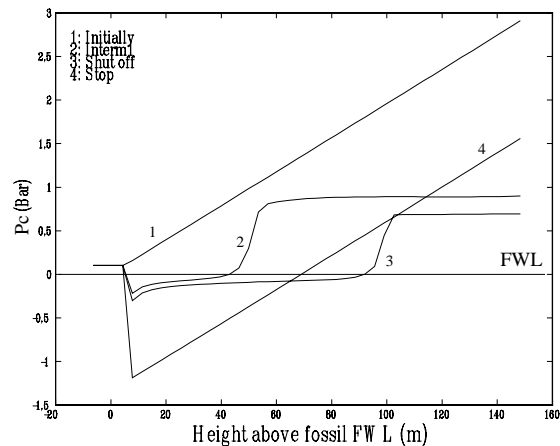


Fig. 12: Capillary pressure development, high rates.

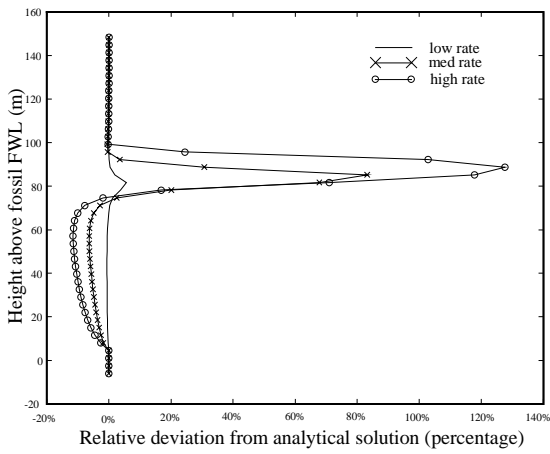


Fig. 13: Relative deviation from ultralow rate solution, Skjæveland's hysteresis model.

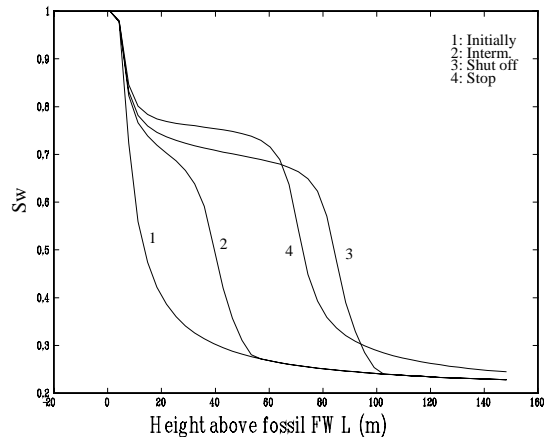


Fig. 16: Saturation distribution at different time levels for medium rate case, Killough's model.

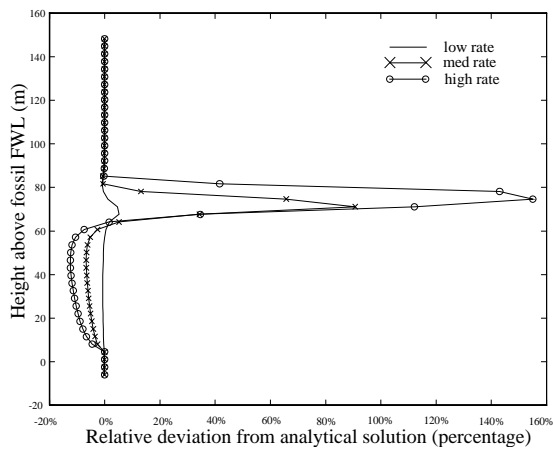


Fig. 14: Relative deviation from ultralow rate solution, Skjæveland's hysteresis model. Compressed transition zone.

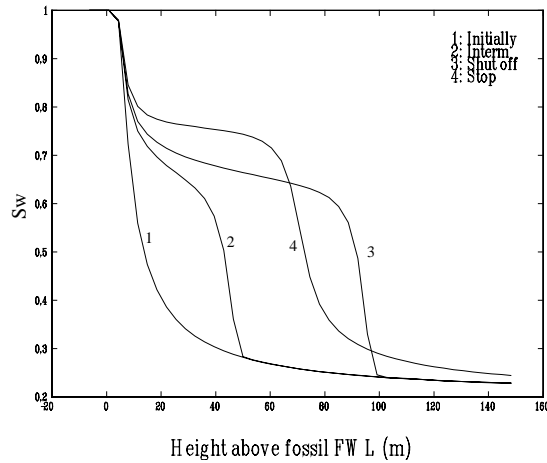


Fig. 17: Saturation distribution at different time levels for high rate case, Killough's model.

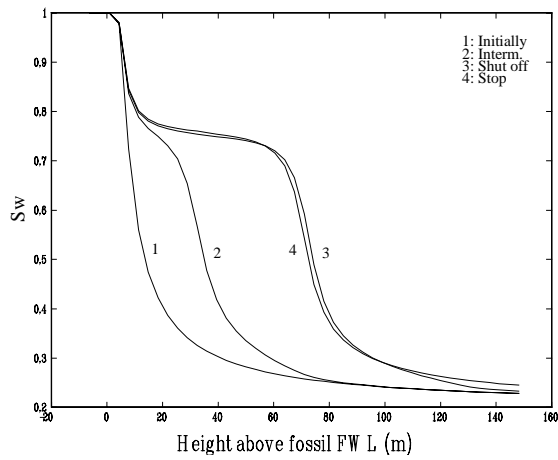


Fig. 15: Saturation distribution at different time levels for low rate case, Killough's model.

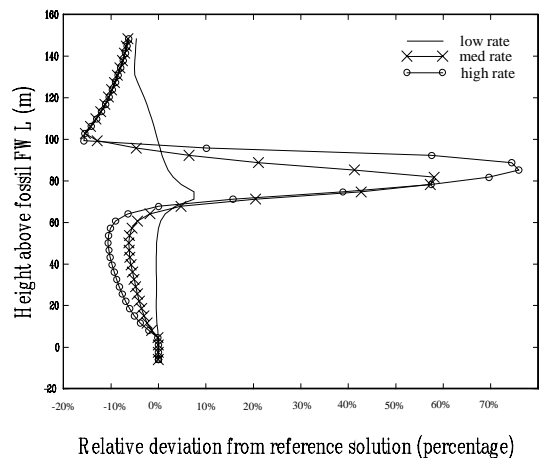


Fig. 18: Relative deviation from from ultralow rate solution at well shut off. Killough's model

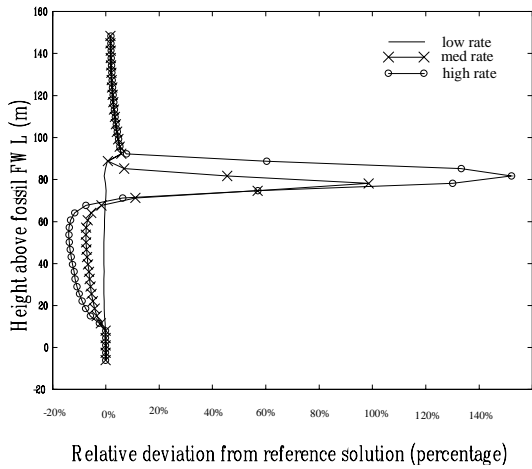


Fig. 19: Relative deviation from ultralow rate for different rates. Compressed transition zone.

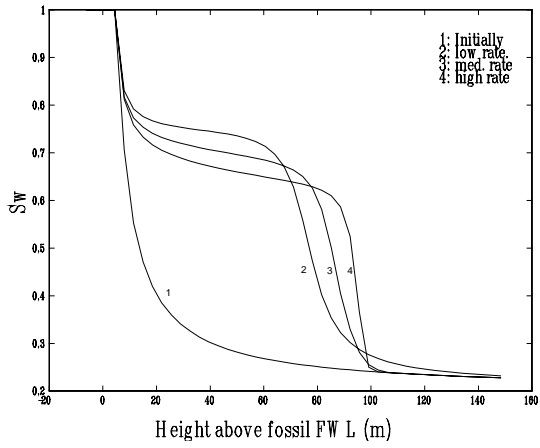


Fig. 20: Front solutions at shut off. Capillary diffusion increases with lower rates.

